Research Article | Vol. 28, No. 1 / 6 January 2020 / Optics Express 40

Optics EXPRESS

Cross-polarization suppression for patch array antennas via generalized Kerker effects

WEISHUANG YIN,[1] XIUYE LIANG,[1] ANG CHEN,[1] ZHE ZHANG,[1] LEI SHI,[1,3] FANG GUAN,[1,2,4] XIAOHAN LIU,[1] AND JIAN ZI[1]

[1]*Department of Physics, Fudan University, Shanghai 200438, China*
[2]*Institute for Nanoelectronic devices and Quantum computing, Fudan University, Shanghai 200438, China*
[3]*lshi@fudan.edu.cn*
[4]*fguan@fudan.edu.cn*

Abstract: The generalized Kerker effect has recently gained an explosive progress in metamaterials, from the scattering management of particle clusters to the reflection and transmission manipulation of metalattices and metasurfaces. Various optical phenomena observed can be explained by the generalized Kerker effect. Due to the same nature of electromagnetic waves, we believe that the generalized Kerker effect can also be used in the microwave field. Inspired by this, in this letter we design a kind of patch array antenna to suppress the cross-polarization by interferences of multipoles. Using different far-field radiation phase symmetries of electromagnetic multipoles for the patch, the cross-polarization can be almost cancelled while the co-polarization be kept. A pair of 8×8 U-slot patch array antennas, working in a wide band (8.8 GHz-10.4 GHz), have been designed, fabricated and measured to verify our proposal. Simulated and measured results both agree well with the theory, showing more than 20 dB gain suppression of the cross-polarization, which indicates the universality of the generalized Kerker effect in electromagnetic waves.

1. Introduction

The generalized Kerker effect [1–7] has extended its original version [8] to various optical phenomena in nanophotonics and meta-optics. The physics underlying the effect can been understood to a large extent by the interference of different electromagnetic multipoles in subwavelength structures [9–13]. Directional scattering of individual particles [14–16], could be induced by interference of electric dipole (ED) and magnetic dipole (MD) modes. Perfect transmission or reflection can be realized in periodic high-index dielectric cylinders [17–19] with excitations of high-order modes, such as electric quadrupole (EQ) and magnetic quadrupole (MQ) modes. In metalattices [20], such interference between multipole modes has been used for higher-order diffraction management. With such great achievements in nanophotonics [21–24], we believe that the generalized Kerker effect can also been applied to antennas [25,26].

Patch antennas are widely used in phased array antenna systems [27] and wireless communication systems [28]. They have advantages of low profile, low cost, light weight and easy fabrication. The patch excited by the dominant TM_{10} mode is inherently a linearly polarized structure. Unfortunately for such patch antennas, an unwanted cross-polarization stemming from TM_{02} mode arises in practice, which is orthogonal to the co-polarization (TM_{10}) [29]. For phased array applications especially, when scanning to larger angle, the cross-polarization becomes even higher than the co-polarization, which would affect the normal use of the arrays. It have found that the cross-polarization is mainly caused by the radiation of high-order modes and currents on the feeding probes [30]. Several methods of suppressing the cross-polarization have been demonstrated, such as employing defected ground structures, feeding the antenna by a dual-probe system with out-of-phase signals [31], using an aperture-coupled feed or a meandering probe

#377577 https://doi.org/10.1364/OE.28.000040
Journal © 2020 Received 11 Sep 2019; revised 29 Nov 2019; accepted 29 Nov 2019; published 23 Dec 2019

Optics EXPRESS

[32] and so on [29]. However, these technologies will either increase the structure complexity or deteriorate other performance of the antennas, such as incurring excessive back radiation.

In this letter, we apply the generalized Kerker effect to suppress the cross-polarization of the patch array antennas by overlapping different multipolar moments within different patch units. A pair of 8×8 patch arrays with probe feeding are built to verify our proposal. One is a normal (general periodically distributed) U-slot patch array, labeled by "Array-NORM" for simplicity; the other is a unit-alternating half-rotated (UAHR) U-slot patch array ("Array-UAHR"). The feeding probes also have very week radiation because the total thickness of the antenna array is deep-subwavelength, say only 0.17λ. Both simulated and measured results show that our proposed wide-angle patch array has an excellent performance for suppressing cross-polarization over 15% bandwidth (8.8 GHz to 10.4 GHz).

2. Theory and design

As schematically shown in Fig. 1(a), a general patch antenna is a sandwich system consisting of a ground plane, a substrate and a patch. It is fed via SMP coaxial connector, where the inner conductor of the coaxial connector is attached to the patch while the outer conductor is connected to the ground plane. In this letter, we analyzed the most common used rectangular patch in detail. The substrate used here is Rogers5880 with a relative permittivity of $\epsilon = 2.2$, and its thickness is 2.5 mm. The patch and the ground are copper and aluminum, respectively. The U-shaped slot machined on the patch aims at broadening the bandwidth of the antenna and modulating the electric fields underneath the patch. Here the multiple cavity modes are used to analyze the patch antenna [33]. A patch antenna can be thought of as an open dielectric-loaded resonant cavity. The open edges are equivalent to radiating magnetic walls, while the patch and ground plane to ideal electrical walls. Such a cavity will support discrete multiple modes similar to those of a fully enclosed metallic cavity.

In this letter, we analyzed the most common used rectangular patch in detail. The theory of characteristic mode (TCM) based on method of moment is widely used in the mode expansion of metasurface antennas [34,35]. Here the TCM is applied to identify the desired modes in our patch antenna system. As shown in Fig. 1(b), the modal significances from 8 to 11 GHz are calculated by the multilayer solver in CST. The first three strongest modes are TM_{10}, TM_{01} and TM_{02}, their fringing field distributions around the U-slot patch are shown in Fig. 1(c). The other higher order modes are so weak that can be neglected. We set the feed point in the center of the patch, where the electric field of TM_{01} mode is close to zero. Therefore, the TM_{01} mode is difficult to be excited. In the subsequent discussion we only consider the two dominant components, TM_{10} and TM_{02}. Of the two, the fundamental mode we preferred is the TM_{10} mode. The fields underneath the patch for these two modes are illustrated in Fig. 2(a), which are denoted by green arrows. Figure 2(b) plots the radiation patterns for the *H*- and *E*-planes respectively. The co-polarization in the *H*- and *E*-planes mainly comes from the radiation of the TM_{10} mode, while the unwanted cross-polarization in the *H*-plane with a dual-peak shape comes from the radiation of the TM_{02} mode. Actually, the electric fields with sine or cosine form in both two modes don't contribute much to far fields due to their oscillatory behaviors, thus cancelling each other along the principal planes. While the electric fields at the other patch edges with equal amplitude would be the primary contributors to the far-field radiation of a patch. We define the *E*-plane and *H*-plane, which are parallel and orthogonal to electric-field vectors respectively, according to the TM_{10} mode. The basic radiating mechanism of the TM_{10} mode can be considered as two radiating slots spaced about $\lambda_g/2$ apart (λ_g is the effective wavelength in the dielectric), equivalent to a magnetic dipole.

The multipolar expansion formalism described by Grahn et al [36,37]. is applied to do a direct calculation of the multipole moments by recording the radiated electromagnetic fields of each mode on a spherical surface with 1 m radius. Figure 2(c) shows the multipole moments

Optics EXPRESS

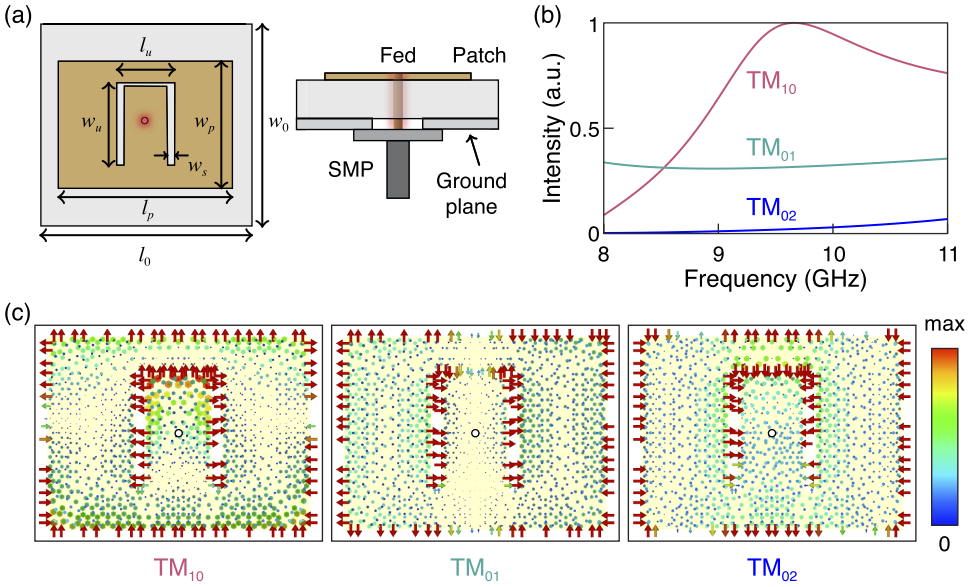

Fig. 1. (a) Illustration of U-slot patch unit. The top view (left panel) shows the structural parameters: l_0 = 14.5 nm, w_0 = 14 nm, l_p = 12 nm, w_p = 8.8 nm, l_u = 4 nm, w_u = 5.5 nm and w_s = 0.5 nm. The side view (right panel) illustrates the corresponding structures. (b) Characteristic modes for the unit cell of the U-slot antenna. Here only three characteristic modes (TM_{10}, TM_{01}, TM_{20}) with the top strongest intensities are shown. (c) Electric near-field distributions of the three modes.

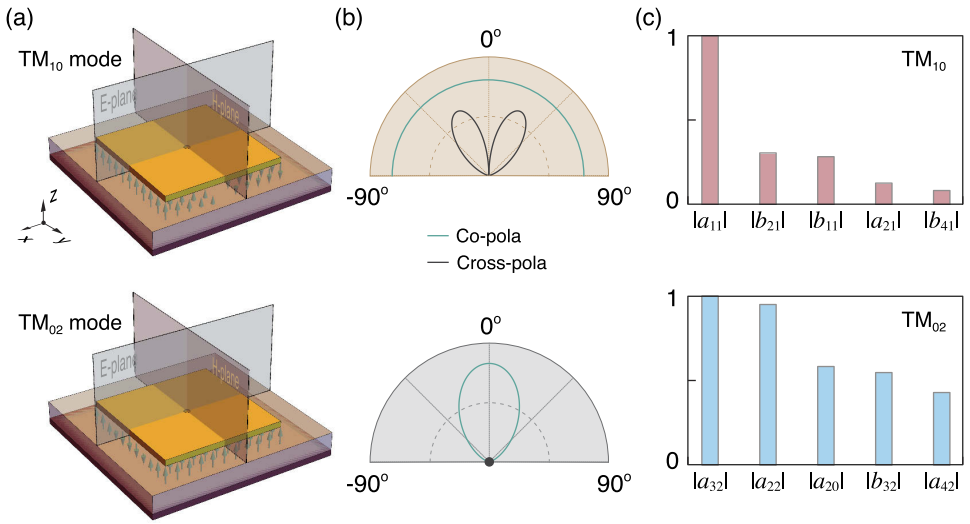

Fig. 2. (a) Fundamental mode (TM_{10}) and second dominant mode (TM_{02}) for a rectangular patch. Green arrows denote the electric fields. *H*- and *E*-planes are defined by TM_{10} mode. (b) Radiation patterns for the *H*- and *E*-planes respectively with exciting the two modes in (a). (c) Normalized expansion coefficients for the two modes.

Optics EXPRESS

with normalized magnitudes of expansion coefficients corresponding to TM_{10} mode and TM_{02} mode, respectively. Here the multipole moments with very small coefficients are not shown. The dominant multipolar component for TM_{10} mode is electric dipole, while TM_{02} mode has been expanded into a series of multipoles. Base on the symmetry difference between the two modes, the multipolar interference can be implemented to suppress the cross-polarization of patch arrays.

3. Simulations and experiments

In order to verify the effectiveness of method for cross-polarization suppression mentioned above, two 8×8 U-slot patch arrays are designed and simulated; see in Fig. 3(a). The impedance bandwidth (VSWR<2) of the patch unit, under the periodic boundary, is more than 15% covering 8.8 GHz-10.4 GHz. It is broadened because of the multi-resonances of the U-slot. The substrate integrated waveguide (SIW) cavity is employed to impede surface waves [38]. All U-slot patch antenna units in the up array align to one direction, while those in the below one rotate 180° alternately between rows, as shown in Fig. 3(a).

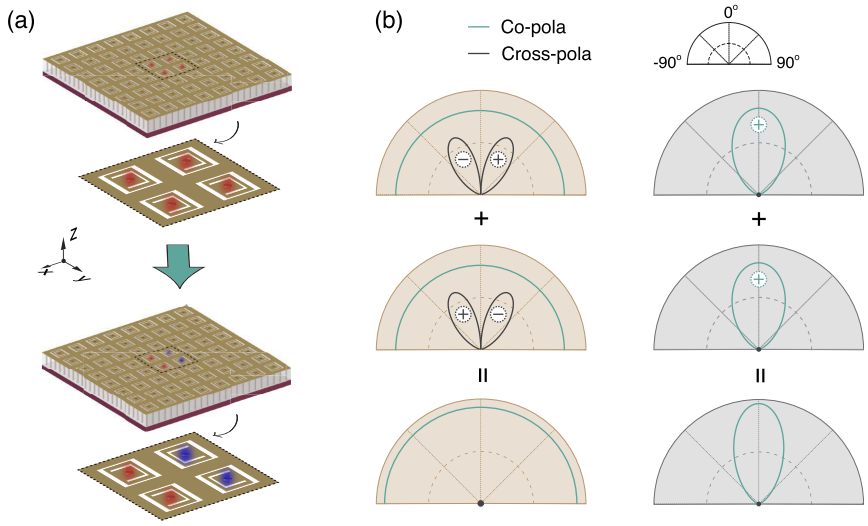

Fig. 3. (a) Schematic view of Array-NORM and Array-UAHR, both with exciting the central four U-slot units. Red and blue give out-of-phase excitations. (b) Phase-symmetry analysis for multipole-mode radiations for Array-UAHR.

For generalized Kerker effects, far-field radiation phase symmetries become essential for the study of multipolar interferences. The total far field radiation of an array antenna is modulated by the interference of all these multipolar components within each single patch antenna. To cancel the radiations of all the multipoles corresponding to TM_{02} mode while protecting the co-polarization is not easy. In our phased array system, we have more degrees of freedom to modulate the phases of the multipoles, either by structure rotating or by out-of-phase feeding. In the subsequent analyses, we will show the interference cases for the ED and EQ components within different antenna elements. This method is also suitable for other higher multipoles of the structure. Figure 3(b) shows schematically the phase-symmetry analysis for electromagnetic multipole-mode radiations for Array-UAHR. The original radiation patterns of an individual patch antenna unit are shown in Fig. 2(b). The cross-polarization level of H-plane is very high, while that of E-plane can be negligible. So we need to suppress cross-polarization of H-plane with simultaneously no influence on the E-plane . If we can feed adjacent patch units with out-of-phase signals, thus the cross-polarization radiated by them will interference destructively

Optics EXPRESS

due to the overlap of the out-of-phase EQ modes. But it should be noted that the far-field phase of ED modes must stay the same, hence leading to constructive interference of the co-polarization. Fortunately, we find that the phases of co-polarization and cross-polarization radiations are of odd and even parities, respectively. When we rotate the patch unit by a half circle, electric fields of EQ mode (cross-polarization) wouldn't be changed, but those of the ED will have a 180° phase inversion, which can be understood by Fig. 2(a). The interference cases for other multipoles are just the same. Thus, by feeding the patch unit out of phase meanwhile rotating the patch unit by a half circle, the co-polarization far-field phase remains unchanged, while that of the cross-polarization have a 180° phase inversion. Based on the discussion above, we can construct a patch array of ultra-low cross-polarization in both *H*- and *E*-plane via generalized Kerker effect by 180° structure rotating and 180° inversion feeding alternately between rows.

Two 8×8 patch arrays are fabricated as depicted in Figs. 4(a) and (b). The measured radiation patterns of four patch units in the arrays center for principal planes are compared with simulated results in Figs. 4(c)–(f). Here we show the broadside radiation patterns, where the maximum gain appear at $\theta = 0°$. For simplicity, we only show the results at 10 GHz. Among them, (c) and (d) are the *H*- and *E*-plane radiation patterns of Array-NORM respectively, while (e) and (f) belong to Array-UAHR. We first discuss the simulated results. The *H*-plane radiation patterns for Array-NORM are plotted in Fig. 4(c), where the cross-polarization is extremely high and forms a dual-peak shape, nearly −10 dB. This corresponds to the EQ radiation shown in Fig. 3(b). As for *E*-plane patterns, the cross-polarization is relatively flat in the whole visual space of the antenna, with 50 dB lower than the co-polarization in the working space of ±60°. Array-UAHR, to which generalized Kerker effect is applied, has comparatively reduced cross-polarization level in *H*-plane, as shown in Fig. 4(e). The simulated cross-polarization reduces more than 20 dB around the broadside direction compared with Array-NORM. The cross-polarization of *E*-plane is almost unaffected, and still remains at a low level. Such simulated results agree well with the theory shown in Figs. 3(b)–(c). Furthermore, because of the ground plane, backward radiation of the array is close to zero, and thus we only show the −90°-90° visible space of Figs. 4(c)–(f), which is the same as −90°-0°-90° section in Fig. 3(b). As we can see, the measured

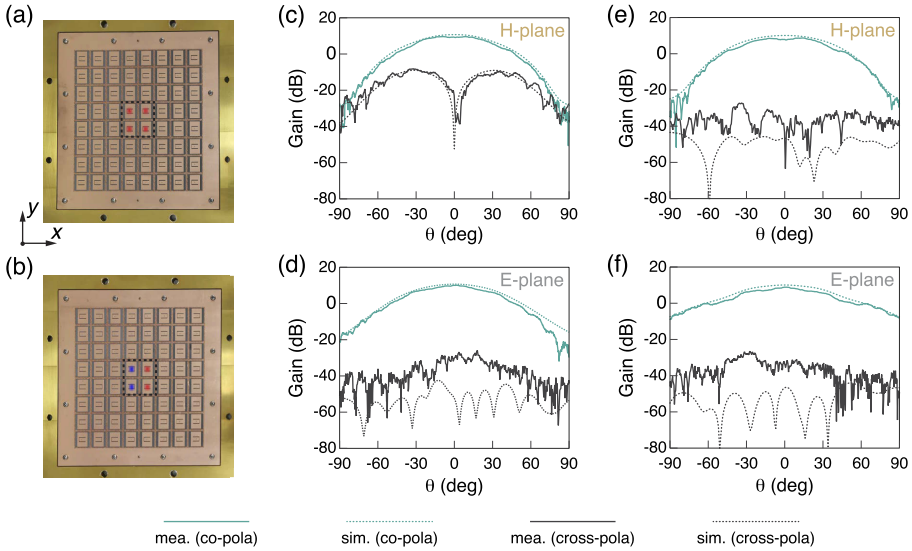

Fig. 4. Optical photos of (a) Array-NORM and (b) Array-UAHR. (c) *H*-plane and (d) *E*-plane broadside (maximum gain appears at 0°) radiation patterns for Array-NORM with exciting the four units in (a)–(b). (e) and (f) for Array-UAHR.

Optics EXPRESS

co-polarization patterns are all in a good agreement with the simulated ones. And the measured H-plane cross-polarization of Array-UAHR is about 20 dB lower than that of Array-NORM at the broadside direction. The vanishment of the dual-peak shape in the H-plane cross-polarization pattern confirms that the multipolar radiations of TM_{02} mode has been cancelled out, verifying the effectiveness of our proposed method.

In order to further confirm the cross-polarization characteristics during angle steering, we simulate the scanning radiation patterns of two aforementioned configurations, as seen in Fig. 5. The main beams of both two array antennas can scan from $-75°$ to $+75°$, the angle θ where maximum gain locates, at 10 GHz with a gain fluctuation less than 4 dB. The patterns of Array-NORM are shown in (c) and (d). As expected, the cross-polarization in H-plane will increase sharply with increasing the scanning angle. And for Array-UAHR, the cross-polarization of H-plane shown in Fig. 5(e) is still very low, about 60 dB lower than the co-polarization even at 75°-scanning and demonstrates its outstanding wide-angle scanning ability with remarkable cross-polarization suppression.

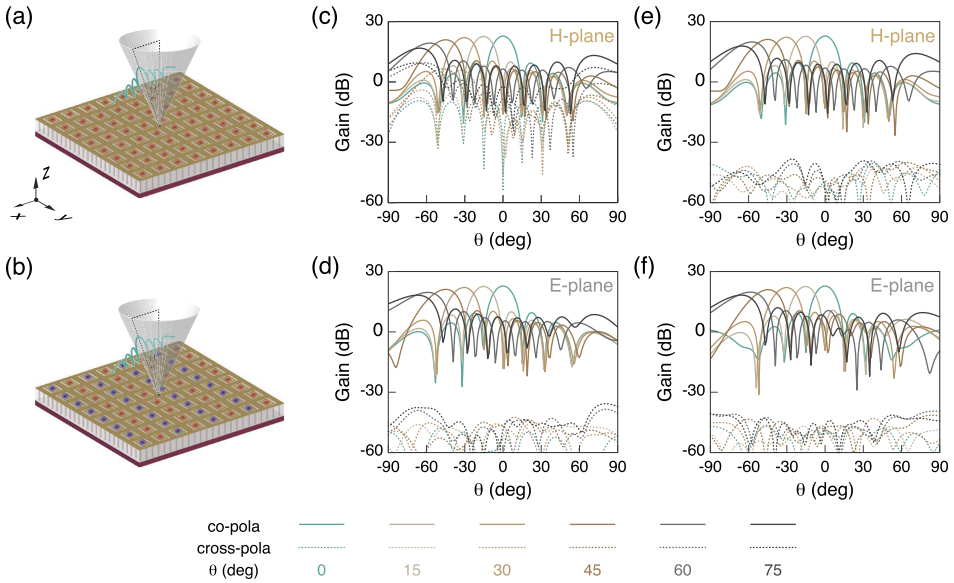

Fig. 5. Schematic views of (a) Array-NORM and (b) Array-UAHR. (c) H-plane and (d) E-plane scanning radiation patterns for Array-NORM. (e) and (f) for Array-UAHR.

4. Conclusion

In summary, inspired by the generalized Kerker effect, a method is proposed, by 180° structure rotating and 180° inversion feeding alternately between rows, to suppress the cross-polarization of patch arrays widely used in detecting and communication systems. The undesired cross-polarization in H-plane coming from the multipolar combinations of the TM_{02} mode reduces dramatically (more than 20 dB), while other performance remains excellent. Meanwhile, good ±75° array scanning performance in both H-plane and E-plane can been maintained. This method shows excellent advantages in manipulating electromagnetic fields, which doesn't need add any extra structures and has little influence on other performance of the array. All the results prove that generalized Kerker effect can be used to guide the antenna design and indicate the universality of the generalized Kerker effect in electromagnetic waves. So we believe that the generalized Kerker effect has opened a door to microwave domain. The effect may be used in

Optics EXPRESS

many practical microwave antenna problems, such as backward radiation suppression, side-lobe suppression, beam shaping, gain enhancement and so on.

Funding

National Basic Research Program of China (973 Program) (2015CB659400, 2016YFA0301103, 2016YFA0302000, 2018YFA0306201); Science and Technology Commission of Shanghai Municipality (17142200100, 17ZR1442300); National Natural Science Foundation of China (11604355, 11727811, 11774063, 91750102).

Acknowledgments

We thank Prof. Wei Liu for the help of multipolar expansion formalism.

Disclosures

The authors declare no conflicts of interest.

References

1. W. Liu and Y. S. Kivshar, "Generalized kerker effects in nanophotonics and meta-optics," Opt. Express **26**(10), 13085–13105 (2018).
2. V. E. Babicheva and A. B. Evlyukhin, "Resonant lattice Kerker effect in metasurfaces with electric and magnetic optical responses," Laser Photonics Rev. **11**(6), 1700132 (2017).
3. K. Hannam, D. A. Powell, I. V. Shadrivov, and Y. S. Kivshar, "Dispersionless optical activity in metamaterials," Appl. Phys. Lett. **102**(20), 201121 (2013).
4. A. E. Krasnok, D. S. Filonov, C. R. Simovski, Y. S. Kivshar, and P. A. Belov, "Experimental demonstration of superdirective dielectric antenna," Appl. Phys. Lett. **104**(13), 133502 (2014).
5. H. K. Shamkhi, A. Sayanskiy, A. C. Valero, A. S. Kupriianov, P. Kapitanova, Y. S. Kivshar, A. S. Shalin, and V. R. Tuz, "Transparency and perfect absorption of all-dielectric resonant metasurfaces governed by the transverse kerker effect," Phys. Rev. Mater. **3**(8), 085201 (2019).
6. A. Pors, S. K. Andersen, and S. I. Bozhevolnyi, "Unidirectional scattering by nanoparticles near substrates: generalized kerker conditions," Opt. Express **23**(22), 28808–28828 (2015).
7. J. Y. Lee, A. E. Miroshnichenko, and R.-K. Lee, "Simultaneously nearly zero forward and nearly zero backward scattering objects," Opt. Express **26**(23), 30393–30399 (2018).
8. M. Kerker, D.-S. Wang, and C. Giles, "Electromagnetic scattering by magnetic spheres," J. Opt. Soc. Am. **73**(6), 765–767 (1983).
9. P. D. Terekhov, K. V. Baryshnikova, A. S. Shalin, A. Karabchevsky, and A. B. Evlyukhin, "Resonant forward scattering of light by high-refractive-index dielectric nanoparticles with toroidal dipole contribution," Opt. Lett. **42**(4), 835–838 (2017).
10. M. Liu, C. Zhao, and B. Wang, "Polarization management based on dipolar interferences and lattice couplings," Opt. Express **26**(6), 7235–7252 (2018).
11. S. D. Isro, A. A. Iskandar, Y. S. Kivshar, and I. V. Shadrivov, "Engineering scattering patterns with asymmetric dielectric nanorods," Opt. Express **26**(25), 32624–32630 (2018).
12. P. Terekhov, H. Shamkhi, E. Gurvitz, K. Baryshnikova, A. Evlyukhin, A. Shalin, and A. Karabchevsky, "Broadband forward scattering from dielectric cubic nanoantenna in lossless media," Opt. Express **27**(8), 10924–10935 (2019).
13. H. K. Shamkhi, K. V. Baryshnikova, A. Sayanskiy, P. Kapitanova, P. D. Terekhov, P. Belov, A. Karabchevsky, A. B. Evlyukhin, Y. Kivshar, and A. S. Shalin, "Transverse scattering and generalized kerker effects in all-dielectric mie-resonant metaoptics," Phys. Rev. Lett. **122**(19), 193905 (2019).
14. M. Neugebauer, P. Woźniak, A. Bag, G. Leuchs, and P. Banzer, "Polarization-controlled directional scattering for nanoscopic position sensing," Nat. Commun. **7**(1), 11286 (2016).
15. I. M. Hancu, A. G. Curto, M. Castro-López, M. Kuttge, and N. F. van Hulst, "Multipolar interference for directed light emission," Nano Lett. **14**(1), 166–171 (2014).
16. J. Li, N. Verellen, D. Vercruysse, T. Bearda, L. Lagae, and P. Van Dorpe, "All-dielectric antenna wavelength router with bidirectional scattering of visible light," Nano Lett. **16**(7), 4396–4403 (2016).
17. W. Liu, "Generalized magnetic mirrors," Phys. Rev. Lett. **119**(12), 123902 (2017).
18. M. Decker, I. Staude, M. Falkner, J. Dominguez, D. N. Neshev, I. Brener, T. Pertsch, and Y. S. Kivshar, "High-efficiency dielectric huygens' surfaces," Adv. Opt. Mater. **3**(6), 813–820 (2015).
19. P. Moitra, B. A. Slovick, W. Li, I. I. Kravchencko, D. P. Briggs, S. Krishnamurthy, and J. Valentine, "Large-scale all-dielectric metamaterial perfect reflectors," ACS Photonics **2**(6), 692–698 (2015).
20. Y. Ra'di, V. S. Asadchy, S. U. Kosulnikov, M. M. Omelyanovich, D. Morits, A. V. Osipov, C. R. Simovski, and S. A. Tretyakov, "Full light absorption in single arrays of spherical nanoparticles," ACS Photonics **2**(5), 653–660 (2015).

Optics EXPRESS

21. M. V. Rybin, D. S. Filonov, K. B. Samusev, P. A. Belov, Y. S. Kivshar, and M. F. Limonov, "Phase diagram for the transition from photonic crystals to dielectric metamaterials," Nat. Commun. **6**(1), 10102 (2015).
22. A. I. Kuznetsov, A. E. Miroshnichenko, M. L. Brongersma, Y. S. Kivshar, and B. Luk'yanchuk, "Optically resonant dielectric nanostructures," Science **354**(6314), aag2472 (2016).
23. N. I. Zheludev and Y. S. Kivshar, "From metamaterials to metadevices," Nat. Mater. **11**(11), 917–924 (2012).
24. I. S. Maksymov, A. R. Davoyan, and Y. S. Kivshar, "Enhanced emission and light control with tapered plasmonic nanoantennas," Appl. Phys. Lett. **99**(8), 083304 (2011).
25. T. Li, H. Yang, Q. Li, C. Zhang, J. Han, L. Cong, X. Cao, and J. Gao, "Active metasurface for broadband radiation and integrated low radar cross section," Opt. Mater. Express **9**(3), 1161–1172 (2019).
26. X. Li, J. Yang, Y. Feng, M. Yang, and M. Huang, "Compact and broadband antenna based on a step-shaped metasurface," Opt. Express **25**(16), 19023–19033 (2017).
27. A. B. Rohwer, D. H. Desrosiers, W. Bach, H. Estavillo, P. Makridakis, and R. Hrusovsky, "Iridium main mission antennasa – phased array success story and mission update," in *2010 IEEE International Symposium on Phased Array Systems and Technology*, (IEEE, 2010), pp. 504–511.
28. X. Gu, D. Liu, C. Baks, O. Tageman, B. Sadhu, J. Hallin, L. Rexberg, and A. Valdes-Garcia, "A multilayer organic package with 64 dual-polarized antennas for 28ghz 5g communication," in *2017 IEEE MTT-S International Microwave Symposium (IMS)* (IEEE, 2017), pp. 1899–1901.
29. K. Woelder and J. Granholm, "Cross-polarization and sidelobe suppression in dual linear polarization antenna arrays," IEEE Trans. Antennas Propag. **45**(12), 1727–1740 (1997).
30. Z. N. Chen and M. Y. W. Chia, "Experimental study on radiation performance of probe-fed suspended plate antennas," IEEE Trans. Antennas Propag. **51**(8), 1964–1971 (2003).
31. D. Guha, M. Biswas, and Y. M. Antar, "Microstrip patch antenna with defected ground structure for cross polarization suppression," IEEE Trans. Antennas Propag. **4**, 455–458 (2005).
32. P. Li, H. Lai, K. Luk, and K. Lau, "A wideband patch antenna with cross-polarization suppression," IEEE Antennas Wirel. Propag. Lett. **3**, 211–214 (2004).
33. C. A. Balanis, *Modern antenna handbook* (John Wiley & Sons, 2011).
34. P. Grahn, A. Shevchenko, and M. Kaivola, "Electromagnetic multipole theory for optical nanomaterials," New J. Phys. **14**(9), 093033 (2012).
35. W. J. Chen, Y. T. Chen, and W. Liu, "Singularities and Poincaré Indices of Electromagnetic Multipoles," Phys. Rev. Lett. **122**(15), 153907 (2019).
36. R. Harrington and J. Mautz, "Theory of characteristic modes for conducting bodies," IRE Trans. Antennas Propag. **19**(5), 622–628 (1971).
37. F. H. Lin, T. Li, and N. Z. Chen, "Recent Progress in Metasurface Antennas Using Characteristic Mode Analysis," *2019 13th European Conference on Antennas and Propagation (EuCAP)* 1–5 (2019).
38. M. H. Awida, A. H. Kamel, and A. E. Fathy, "Analysis and design of wide-scan angle wide-band phased arrays of substrate-integrated cavity-backed patches," IEEE Trans. Antennas Propag. **61**(6), 3034–3041 (2013).